HHS Public Access

Author manuscript

Biomaterials. Author manuscript; available in PMC 2018 April 01.

Published in final edited form as:

Biomaterials. 2017 April ; 124: 169–179. doi:10.1016/j.biomaterials.2017.02.002.

Exploring Deformable Particles in Vascular-Targeted Drug Delivery: Softer is Only Sometimes Better

Margaret B. Fish[1], **Catherine A. Fromen**[1], **Genesis Lopez-Cazares**[1], **Alexander W. Golinski**[1], **Timothy F. Scott**[1,3], **Reheman Adili**[4], **Michael Holinstat**[4,5], and **Omolola Eniola-Adefeso**[1,2,3,*]

[1]Department of Chemical Engineering, University of Michigan, Ann Arbor, MI 48109

[2]Department of Biomedical Engineering, University of Michigan, Ann Arbor, MI 48109

[3]Macromolecular Science and Engineering Program, University of Michigan, Ann Arbor, MI 48109

[4]Department of Pharmacology, University of Michigan, Ann Arbor, MI 48109

[5]Department of Cardiovascular Medicine, Samuel and Jean Frankel Cardiovascular Center, University of Michigan, Ann Arbor, MI 48109

Abstract

The ability of vascular-targeted drug carriers (VTCs) to localize and bind to a targeted, diseased endothelium determines their overall clinical utility. Here, we investigate how particle modulus and size determine adhesion of VTCs to the vascular wall under physiological blood flow conditions. In general, deformable microparticles (MPs) outperformed nanoparticles (NPs) in all experimental conditions tested. Our results indicate that MP modulus enhances particle adhesion in a shear-dependent manner. In low shear human blood flow profiles *in vitro*, low modulus particles showed favorable adhesion, while at high shear, rigid particles showed superior adhesion. This was confirmed *in vivo* by studying particle adhesion in venous shear profiles in a mouse model of mesenteric inflammation, where MP adhesion was 127% greater ($p<0.0001$) for low modulus particles compared to more rigid ones. Mechanistically, we establish that particle collisions with leukocytes drive these trends, rather than differences in particle deformation, localization, or detachment. Overall, this work demonstrates the importance of VTC modulus as a design parameter for enhanced VTC interaction with vascular walls, and thus, contributes important knowledge for development of successful clinical theranostics with applications for many diseases.

*Corresponding author: Omolola Eniola-Adefeso, Department of Chemical Engineering, University of Michigan, NCRC B028/Rm. G046W, 2800 Plymouth Road, Ann Arbor, MI 48109, Telephone: (734) 936-0856, lolaa@umich.edu.

Conflict of interest statement: The authors have declared that no conflict of interest exists.

AUTHOR CONTRIBUTIONS

M.B.F., C.A.F., T.F.S., R.A., M.H., and O.E.A. designed research; M.B.F., C.A.F., G.L., and A.W.G. performed experiments; M.B.F., C.A.F., and R.A. contributed new reagents/analytic tools; M.B.F., C.A.F., G.L., and A.W.G. analyzed data; and M.B.F., C.A.F., T.F.S., R.A., M.H., and O.E.A. wrote the paper.

Keywords

Hydrogel; Modulus; Deformability; Vascular-Targeted Carrier; Shear Force; Hemodynamics

INTRODUCTION

Vascular-targeted drug carriers (VTCs) are particles designed to exploit differential surface protein expression in diseases involving the endothelium, for an increase in drug localization and corresponding decrease in off-target toxicity. The development and clinical approval of VTC systems could revolutionize the treatment of many common but therapeutically challenging diseases, including cancer and cardiovascular diseases. Recent consideration of VTC physical properties, including size, shape, and surface charge[1–5], has improved historically low targeted drug delivery efficiency. More recently, researchers have also explored the impact of particle stiffness, demonstrating that lower modulus particles have increased circulation time *in vivo,*[6–9] attributed to both a slower rate of particle phagocytosis and decreased mechanical filtration in the kidney and spleen.[10–12] The work presented here integrates these two lines of research to present a comprehensive study of the critical role of particle modulus on VTC targeting efficiency.

As VTCs traverse the vasculature, they must navigate complex blood flow to contact the endothelium, otherwise all targeting functionalities are negated. In blood flow, cells segregate into a concentrated red blood cell (RBC) core in the center, while white blood cells (WBCs) and platelets are excluded to the RBC- free layer (RBC-FL) to interact with endothelial cells (ECs). Hydrodynamic, heterogeneous collisions between blood components drive this segregation in flow.[13–16] The differences in cellular size and stiffness are often used to explain WBC and platelet margination, which, by definition, is the localization to ECs from bulk blood flow. RBCs have a Young's modulus of 26 ± 7 kPa; WBCs are an order of magnitude stiffer than RBCs and platelets are 2–5 times more rigid than RBCs.[17–20] It is vital that VTCs mimic this cellular margination process to interact with the designated endothelium and target effectively *in vivo.* One way to achieve this is to control VTC size. Previous work has shown that optimal VTC size depends on the physical blood properties[21,22]; in human blood, 3 μm is the ideal diameter for spherical, rigid particles to maximally marginate to ECs as determined in *in vitro* flow assays.[23,24] Furthermore, rigid nanoparticles (NPs) demonstrate inefficient margination compared to microparticles (MPs) due to decreased localization to the vessel wall, resulting in low adhesion overall to targeted ECs.[23,25] Unfortunately, rigid MP VTCs may cause deleterious capillary occlusions and are impractical for clinical use. Thus, there is strong motivation to explore a modulus range of both MPs and NPs, with interest to circumvent possible capillary occlusions by MPs and to improve the poor margination dynamics of rigid NPs. Recent studies with varying modulus particles focus on the impact of particle modulus on *in vivo* circulation time, which does not necessarily translate to targeted adhesion.[7] There is a lack of research directly comparing an entire range of particle sizes and physiologically relevant VTC moduli for vascular targeting; there is a critical need for well-designed experiments to fill this gap.

To address this deficiency in the research field, we explore two sizes of four polyethylene glycol (PEG)-based VTCs with a range of Young's moduli, spanning an order and a half of magnitude, including one modulus similar to that of WBCs and one to that of RBCs. We explore how particle modulus and size collectively dictate VTC efficacy based on a range of physiological blood flow conditions, by using particles fabricated with well-controlled surface ligand properties. Our data demonstrate that VTCs cannot be designed as "one size fits all", but rather, require the deliberate selection of VTC modulus based on known hemodynamics of the disease state. Importantly, this is the first study to report how VTC modulus directly affects the final, targeted adhesion of particles both *in vitro* and *in vivo,* providing an exciting and unique perspective on VTC engineering with potential to influence the future VTC system development.

RESULTS

Characterization of PEG-based hydrogel particles

We systemically varied fabrication conditions to synthesize hydrogel particles of varying modulus, as detailed in Fig. 1. Reaction conditions for the PEG hydrogels are detailed in the Supplemental Information; we decreased the moduli from A to D by decreasing the hydrogel cross-linking density. The synthetic scheme for hydrogel polymerization is shown in Fig. 1A–B. The *in situ* polymerization of hydrogel conditions B–D is shown in Fig. 1C. Hydrogel condition A was omitted, as it was too rigid for the *in situ* rheometry. Complete polymerization for each condition, determined from the plateaus in the *in situ* polymerization curves, was achieved within several seconds; indeed, the onset of gelation was so rapid that the precise gel point, as determined by the crossover of the storage (G') and loss (G'') moduli,[26] could not be ascertained (Fig. S1). We utilized a large excess of photoinitiator to ensure maximal polymerization; any unpolymerized monomer was washed out of the swollen hydrogels bulk samples and particles. As VTCs are employed in aqueous conditions of media or blood, the most relevant particle parameter is the swollen shear modulus, which varied over 1.2 orders of magnitude from 170,000 ± 40,000 Pa for condition A to 7,700 ± 300 Pa for condition D (Fig. 1D). By design, hydrogel C closely matches WBC moduli while hydrogel D matches that of RBCs. The equilibrium swelling ratio (ESR, Fig. 1E) is the characterization of the swelling properties of each bulk material type, is shown in both water and human blood plasma. When comparing hydrogel ESR in plasma and water, only hydrogel D showed a significant difference with $p<0.0001$. There were significant differences in ESR when comparing A with B–D. Fig. 1F details the calculated density, pore size, and young's modulus of each hydrogel type.[27]

Having characterized the bulk materials, hydrogel particles of either 2 μm or 500 nm in diameter were fabricated, using the conditions shown in Fig. 1F. Fig. S2 is a schematic of the hydrogel particle fabrication protocol as further explained in the supplemental methods. Resulting particles were sized using dynamic light scattering (DLS) and scanning electron microscopy (SEM). Fig. 2A details the resultant zeta potential (ZP) for all particle conditions, ranging from −23 mV to −32 mV, attributable to the 2-carboxyethyl acrylate (CEA) incorporated into the polymer backbone. Fig. 2B–C show representative SEM images of hydrogel particles; the clustering is a function of being dried for imaging. Particles within

both size groups were found to be spherical and reasonably monodisperse after purification. There were no notable differences observed between particle A and D morphology as demonstrated in the scanning electron micrographs in Fig. 2D–E.

Phagocytic uptake of particles *in vitro* is a predictive technique of particle clearance rate *in vivo.* In general, cells phagocytose rigid particles more rapidly than more deformable counterparts.[7,11] THP-1 uptake of both 500 nm and 2 μm hydrogels of all particle conditions confirmed previously observed trends in the literature, specifically that rigid particles were more readily phagocytosed, and thus, the rate of particle uptake by THP-1 cells decreased from particle A through particle D (Fig. S3).

Modulus dictates hydrogel particle binding under shear *in vitro*

We first evaluated the impact of VTC deformability on adhesion to an inflamed EC monolayer from human blood flow in a parallel plate flow chamber (PPFC) to mimic binding in a human blood vessel. Human umbilical vein EC (HUVEC) monolayers were prepared and activated with interleukin 1β (IL-1β). Hydrogel (A–D) and control polystyrene (PS) particles were conjugated with ~1,000 sialyl Lewis^A (sLe^A) sites/μm^2 (gating shown in Fig. S4). SLe^A is a carbohydrate that has high affinity for E-selectin, a molecule that is upregulated on EC monolayers during inflammation and is minimally expressed on healthy ECs. Particle adhesion density was evaluated at varying wall shear rates (WSRs) (see Eqn. 1 in Methods) that represent a physiological range encountered in human vasculature.

The human blood flow adhesion of sLe^A-coated, 2 μm rigid PS and deformable hydrogel particles is shown in Fig. 3A – C for WSRs of 200, 500, and 1,000 s^{-1}, respectively, with a particle concentration of 1×10^7 particles/mL. At 200 s^{-1}, 2 μm particle adhesion significantly increased with decreasing hydrogel modulus, with particles C and D showing a significant increase in adhesion (p=0.037 and 0.029, respectively) relative to the most rigid hydrogel particle, A. Adhesion of all hydrogel particles was not significantly different when compared to the PS control. At the intermediate WSR of 500 s^{-1}, there was no significant trend amongst the 2 μm hydrogel particles or PS control. However, at the high WSR of 1,000 s^{-1}, the 2 μm hydrogel adhesion trend flipped relative to the low shear trend; the more rigid hydrogel MPs adhered better than low modulus MPs. Hydrogel A showed significant 2.8 and 4.8 fold increases over C and D, with p=0.005 and 0.0008, respectively. The adhesion levels for particles C and D were also significantly lower than the adhesion of the PS control particles.

We then probed the importance of size on the observed trends in our PPFC adhesion assays. Particles of the equivalent moduli, but of 500 nm diameter, were evaluated in the same manner. Notably, a minimum concentration of 1×10^8 particles/mL was necessary in order to observe significant particle adhesion, which is an order of magnitude larger than the concentration evaluated for 2 μm particles. At all WSRs, the rigid PS control performed significantly better than all hydrogel particle types (Fig. 4). There were no significant differences amongst the 500 nm hydrogel particles.

For both particle sizes, increasing the WSR resulted in increased total particle adhesion. However, at higher WSR, more particles travel through the PPFC in the fixed 5 min

experiment time, thus, adhesion trends were normalized by the total number of particles perfused thorough the PPFC, resulting in adhesion efficiency shown in Fig. S5. From these results, we observe that even at a lower particle concentration, 2 μm particles were significantly more efficient in PPFC experiments compared to 500 nm particles, as was previously shown with PS.[23] For MPs, more rigid particles maintained their adhesion efficiency with increased WSR, while adhesion efficiency significantly decreased for the low modulus conditions at higher WSRs. Together, these data indicate that targeted vascular wall adhesion of low modulus hydrogel MPs is heavily dependent on the imposed local blood flow WSR, which is physiologically pertinent, as blood shear varies widely throughout the body.

Low modulus particles produce superior adhesion *in vivo*

To confirm our *in vitro* trends, we next visualized actual targeted particle adhesion, in real time, to inflamed endothelium *in vivo* using a model of acute mesentery inflammation. Topical TNF-α results in inflammation and corresponding P-selectin expression within minutes of stimulation.[28,29] We explored extreme modulus conditions A and D and both particle diameters, 2 μm and 500 nm. All particles types were conjugated with the same surface density of anti-CD62P to ensure rapid, firm adhesion to the inflamed endothelium. Fluorescent hydrogel particles were dosed by equivalent mass and tracked real-time with fluorescent intravital microscopy. An experimental schematic is shown in Fig. 5A, with representative images of 2 μm particle binding in mouse mesenteric veins shown in Fig. 5B. All particles observed were firmly adhered to the inflamed mesenteric vein ECs due to the chosen ligand kinetics. Fig. 5C shows the adhesion number of each particle type, scaled by the number of particles injected and the surface area of the examined vessels. Minimal adhesion of targeted hydrogels was observed in non-inflamed vasculature, as shown in Supplemental Video 1. Overall, the 2 μm particles adhered significantly more than the 500 nm particles, in line with our *in vitro* adhesion efficiencies. Fig. S6 shows the number of each bound scaled by just the vessel surface area; particles were dosed by mass, corresponding to 64.5 times more NPs than MPs, yet NP particle adhesion by number was at most only 14 times more than MP adhesion by number. Thus, MPs demonstrated superior targeted particle adhesion than NPs for targeted applications *in vivo*. Interestingly, within both particle sizes, hydrogel D significantly outperformed hydrogel A, with observed increases of 127% ($p<0.0001$) and 627% ($p=0.002$) for 2 μm and 500 nm, respectively. These results correspond to the trend observed *in vitro*; in the low WSR of the mesentery vein, particle D of lower modulus resulted in improved adhesion over stiffer particle A. High shear arteries were not evaluated *in vivo*, as the flow is pulsatile, and hence, not comparable to the *in vitro* laminar studies. Additionally, large high WSR arteries are not amenable to real-time intravital imaging, and thus, can only be evaluated posthumously, which represents widely varying conditions from those studied *in vitro*.

Evaluation of hydrogel deformability under physiological shear forces

We next sought to identify the major interactions driving the observed particle adhesion trends. Given that NPs showed low adhesion efficiency both *in vitro* and *in vivo* compared to MPs, we focused the subsequent evaluation to 2 μm particles. We investigated the bulk properties of each hydrogel material (A–D) under controlled rheometry shear inputs to

estimate changes in hydrogel particle deformation produced by blood flow (Fig. 6A). The input forces translate to the WSRs of our PPFC experiments, where 0.8 Pa and 4.0 Pa correspond to WSR 200 s^{-1} to 1,000 s^{-1}, respectively. Fig. 6A shows deformation responses linearly increasing with applied force. This linearity was maintained over a larger range of shear force applied by the rheometer (Fig. S7). Interestingly, the percent difference in strain between materials remained constant; material A deformed between 12–14% of the strain of hydrogel D at all applied shears, meaning there is a difference in how these particles will deform in fluid shear near the vascular wall. However, at the most physiologically extreme condition the magnitude of the % strain was less than 0.2%, indicating minimal deformation. These bulk property results were supported by our finite element analysis (FEA). We utilized the Taylor deformability parameter (Δ, defined in SI) as a way to quantify to FEA-modeled deformations. Particles A–D demonstrate minimal deformation within physiological fluid shear profiles, with FEA results showing indiscernible differences in particle shape and height (Fig. 6B, force diagram in Fig. S8). Particle deformation results in a slight shrinkage of the particle height, meaning particle D will be shorter than particle A.[30,31] FEA modeling shows that these changes in height are small compared to the overall size of the particle, with Δ = 0.002 corresponding to only an 8.02 nm decrease in particle D height at a WSR of 1,000 s^{-1} (4 Pa). This is in comparison to a 7.95 nm height decrease in particle A at the same shear rate (Δ =0.001993). Shear stresses of greater than 1,000 Pa would be needed to observe larger differences in deformation between particles; the most extreme condition presented in Fig. 6B at 10 kPa results in a Δ=0.0039 for particle A and Δ=0.05 for particle D, corresponding to a decrease in height of 12.6 and 116 nm, respectively. Thus, these particles have the potential to significantly deform in shape due to shear forces, but do not exhibit these changes during fluid flow shears in our physiological system. To visualize the degree of particle deformation, element displacement of the inset sphere has been amplified by 2x. Thus, the continuous hydrogel particles studied here demonstrate surprisingly small changes in their physical dimensions due to fluid induced shears, indicating that this phenomenon does not significantly contribute to the shear-based adhesion trends.

Next, we analyzed particle localization to the vessel wall from human blood flow using confocal microscopy to determine if differential particle distribution causes the variation in wall adhesion. Fig. 6C shows the *in vitro* localization of each 2 μm hydrogel MP type A–D. Confocal images were taken at the wall of a PPFC while a mixture of human blood and particles were perfused. Fig. 6C shows no significant differences between the wall localization of 2 μm hydrogel particles across the four moduli and three WSRs explored. These results indicate that differences in moduli did not translate to experimentally detectable changes in particle distribution to the wall from blood flow.

Another possible mechanism that could drive trends in PPFC adhesion by modulus is the adhesive force of hydrogel particles once present on the EC monolayer. This is indirectly represented in our data by the rate of attachment of 2 μm particles (Fig. 6D). This plot displays the adhesion over time, captured every 30 secs, for each particle A–D at 1,000 s^{-1} WSR. A mixture of particles and blood were perfused through the PPFC for the first 5 mins, after which, solely buffer was perfused. Fig. 6D shows that for all 2 μm hydrogel particles A–D, there was a linear region of attachment, with only particle A showing detectable

detachment in the 10 mins of buffer only flow. The rates of attachment for the other two WSRs are shown in Fig. S9. The linear rate of attachment indicates dominating adhesion forces. Furthermore, this data demonstrates that even at our highest WSR, no significant number of hydrogel particles detached once adhered to the inflamed EC monolayer.

Removal of white blood cells eliminates adhesion trends

Given that discrepancies in particle deformation, localization, and rate of attachment did not together account for the observed significant trends in particle adhesion, we hypothesized that collisions with WBCs within the RBC-FL may contribute to the experimental phenomena. Importantly, WBCs will be present for all clinically relevant applications of VTCs, yet, we explored their removal from blood flow to better explain the shear dependence of hydrogel adhesion. We repeated PPFC experiments for 2 μm particles as in Fig. 3, but with WBC depleted blood (RBC+plasma). With this blood medium, particle margination remains the same, while interactions between cells and particles within the RBC-FL are removed. As shown in Fig. 7A–C, there were no significant differences in adhesion amongst the hydrogel particle types at any WSR. This lack in adhesion trend compared to the whole blood experiments indicates that WBCs in the RBC-FL have a clear impact on targeted particle adhesion. To determine whether WBCs enhance or reduce particle adhesion, we subtracted RBC+plasma particle adhesion from that in whole blood (Fig. 7D–F). In these plots, positive values denote that particle adhesion was greater in whole blood than in RBC+plasma, indicating that WBCs enhance particle adhesion; negative values indicate that WBCs reduced particle adhesion. WBCs in the RBC-FL had minimal to no impact on PS particle adhesion in low to intermediate shear but significantly enhanced PS adhesion at high WSR of 1,000 s^{-1}. WBCs in the RBC-FL had either a neutral or enhancing impact on hydrogel particle adhesion. At 200s^{-1} (Fig. 7D), WBCs had limited influence on hydrogels A and B, but enhanced particle adhesion for hydrogel particles C and D. At 500 s^{-1} (Fig. 7E), WBCs enhanced particle adhesion for all hydrogel particles in a similar magnitude. A trend becomes pronounced at high shear (1,000 s^{-1}; Fig. 7F), where collisions with WBCs in the RBC-FL helped rigid particles more than low modulus particles. Overall, the impact of WBCs in the RBC-FL was similarly shear dependent as adhesion trends in whole blood medium. Therefore, we can conclude that collisions with WBCs in the RBC-FL prescribe VTC adhesion trends by modulus.

DISCUSSION

To date, no study has extensively evaluated the mechanism by which particle modulus affects vascular targeting, particularly adhesion in blood flow. As a crucial physical property of VTCs, this work suggests the importance of tuning the particle modulus based on local hemodynamics and provides exciting insights aimed at improving translation of VTC systems from the bench top to bedside. Our findings demonstrate the significance of fluid shear in prescribing the ideal modulus for micron-sized particles, shedding light on the importance of understanding physical transport mechanisms in the design of a VTC system. Previous computational work has predicted that the margination dynamics of particles of varying moduli will differ greatly.[19] While varied moduli particles have been explored for theranostic delivery applications *in vivo*[6,8,32–37], no study has directly evaluated the

experimental margination and adhesion propensity of VTCs of varied moduli. Moreover, many previous studies focus on a comparison between two particle moduli and the impact of particle modulus on *in vivo* circulation time, cellular uptake, and tissue biodistribution, which do not necessarily translate to targeted adhesion.[7] There is a critical need to thoroughly evaluate the impact of VTC modulus on the relevant biological transport and adhesion processes to maximize the benefits of vascular-targeted drug delivery.[5,38,39]

In this work, a range of particles (A–D) was fabricated using varied amounts of crosslinked PEG. PEG is routinely utilized in a wide range of biomedical applications for its known resistance to protein fouling, hydrophilicity, biocompatibility, and modularity for fabricating scaffolds with a custom range of moduli and functionalities.[40,41] Of note, covalently polymerized PEG particles are known to be highly stable under physiologic conditions.[42] Many studies have utilized PEG or derivatives to develop drug delivery vehicles, ranging in diameter from 30 nm[43] to over 10 μm and with Young's moduli as low as 200 Pa to as high as 3 MPa.[7,8,44] Furthermore, others have demonstrated that measurements of bulk hydrogel modulus is representative of the corresponding individual MP moduli, hence, our bulk rheometry can be used as a representation of our particle properties.[27] The bulk materials are well characterized in Fig. 1 showing *in situ* rheometry, swollen rheometry, ESRs, and calculated bulk properties. Shown in Fig. 1E, hydrogel D was the only material to exhibit differences in swelling between blood plasma and water, likely due to both the fact that D is the least cross-linked material and blood plasma has a higher osmolarity than water, thereby producing less swelling.[45] Our particles have well-characterized surface ligand densities, ensuring that all conclusions made here are due to physical properties rather than discrepancies in VTC surface ligand presentation. PS was included in *in vitro* assays as an extremely rigid control for the varied moduli hydrogel particles, with an Elastic modulus of about 2 GPa, over 4 orders of magnitude more rigid than hydrogel A.[46] However, we recognize that PS has different material properties than PEG, including increased hydrophobicity,[47] zeta potential, and more; it is well known that PS particles rapidly associate with and are taken up by phagocytes. Furthermore, these extremely rigid particles are known to occlude capillaries, particularly in the lung.[48] Lack of biocompatibility and these differences led to our exclusion of PS from *in vivo* experiments, where this would be most pronounced.

Our *in vitro* and *in vivo* adhesion results indicate that hydrogel MP VTCs are better suited for vascular adhesion than equivalent NP carriers. This corresponds to previously published studies with rigid particles, finding that micron-sized VTCs provide significantly superior vessel wall localization and EC adhesion compared to nano-sized. This is explained by superior exclusion of micron-sized particles out of the RBC-FL, similar to the reported near wall excess of white blood cells,[14,15] while nano-sized particles are suggested to co-localize with RBCs in the center of flow.[23,49] Previous work has demonstrated that deformable MPs can lead to increased circulation time and safe navigation of the vasculature.[8] Indeed, *in vivo* we did not observe tissue entrapment or capillary occlusion of 2 μm hydrogel particles, as has been shown with PS particles in the past.[48] Thus, our results demonstrate the utility of hydrogel MPs specifically for vascular targeting applications, combining improvements in both safety and efficiency. Overall, our results indicate that contributions of particle

deformability and size, as well as the hemodynamics in the target vessel, dictate VTC targeting success.

For both sizes *in vivo*, particle D provided significantly elevated adhesion to the inflamed mesentery wall, compared to more rigid particle A (Fig. 5C). Supplemental Video 1 shows minimal adhesion of targeted particles to non-inflamed mesenteric vasculature via fluorescent intravital microscopy. These results align with a recent comparison of 200 nm targeted particles with moduli of 10 kPa and 3 MPa, which showed improved targeting *in vivo* of the softer formulation.[7] A prevailing explanation for these trends suggests softer particles exhibit longer circulation time, leading to more opportunities to adhere to the target site. Indeed, it has been widely shown that lower modulus particles circulate longer *in vivo*, for their ability to avoid filtration and phagocytosis, as confirmed by our THP-1 uptake trends.[7,8,11,42,43] From our *in vivo* results alone, we cannot rule out this theory, as it is inherently challenging to decouple circulation time from particle modulus. However, our *in vitro* PPFC assay enables isolation of other physical factors, and supports the role of other contributing mechanisms at play.

Our *in vitro* work exposes an interesting phenomenon that the optimal modulus for 2 μm VTC adhesion is heavily dependent on the local shear profile. We utilized WSRs of 200, 500, and 1000 s^{-1}, which represent a physiological range of blood flow found in human post capillary venules and arterioles.[50,51] Namely, lower modulus PEG particles adhere with a higher efficiency compared to more rigid counterparts at low WSRs (200 s^{-1}), which was observed both *in vivo* in the inflamed mesentery model (Fig. 5C) and *in vitro* in the PPFC assay (Fig. 3A, 4A). However, at high shear, the softer particles lose this adhesion advantage. Interestingly, the lower modulus particles, C and D, behave like adherent WBCs, which also adhere less efficiently under high WSR compared to low WSR conditions.[52] These results are anticipated to be highly valuable for the engineering of VTCs; improving targeted adhesion by deliberately electing a particle modulus will facilitate the development of more efficient VTC systems.

We hypothesized that a mix of different phenomena, such as individual particle deformation at the wall, localization efficiency, particle adhesion strength, and collisions with WBCs may each contribute to collectively determine the VTC efficacy by modulus. Minimal particle deformation under fluid shear flow unifies many of these results. According to our FEA simulations, minimal changes in particle deformation and height occurred for the hydrogels in flow, on the order of 8 nm or 0.4% of total diameter for particle D at the highest physiological WSR. This maximal deformation is small, with differences lacking between particle types. This indicates that particle deformation while in flow was not responsible for driving observed differences in vascular wall adhesion *in vitro*. Furthermore, the minimal deformation explains the lack of difference in localization amongst all particle types.[19,31] Deformable particles anti-marginate towards the centerline of flow, while more rigid particles marginate towards the chamber wall.[19,53] In order to produce observable differences in margination, particles must be highly deformable with capillary number (*Ca)* on the order of 0.3. Notably, a large *Ca* denotes a deformable particle, while smaller denotes a rigid particle; most computational papers assign Ca=0.3–0.5 for the “deformable particle” and Ca<0.2 for rigid particles.[19,30] The *Ca* for particle D, presumed as the largest, is

5.2×10^{-4}, a full 3 orders of magnitude smaller than the commonly studied and simulated range of modulus, indicating that particle deformation drives margination.

These results were initially unexpected; we had hypothesized that particles C and D would behave like WBCs and highly deformable RBCs, respectively, because of their matched bulk moduli. Yet, our particle C did not outperform particle D in all conditions studied. While cells are highly deformable, they are typically characterized by surface moduli and internal viscosity, rather than a uniform modulus. Conversely, hydrogel particles are considered as a continuous polymerized matrix and much better represented with a bulk, elastic modulus. This physical difference leads to particles, which, while not rigid, do not deform to the same extent as cells in fluid shears alone. However, other aspects of our study, in line with others' previous results, demonstrate that this range of particle modulus still has a considerable impact on cellular interactions and dynamics in flow. Continuous hydrogel particles of this moduli range have considerably increased circulation time *in vivo*,[8,9] indicating the capacity to deform through narrow capillaries, as well as avoid immune clearance. Indeed, in our work, THP-1 phagocytic cells showed slower uptake rate of lower modulus particles, despite having proved that their shape does not significantly change in fluid flow (Fig. S3). Furthermore, we observed evidence of particle deformation following adhesion at the vascular wall; the most rigid hydrogel A was the only particle that experienced noticeable detachment, designating weaker adhesive forces versus the other hydrogel particle types. Elongated, bound particles experienced a lower removal shear force once wall contact is made, as they were able to minimize their profile protruding in the direction orthogonal to blood flow and capitalize on increased adhesive bonds. Notably, the ligand-receptor pair chosen for these experiments is considered a catch-bond, which prolongs bond lifetime under increased shear force conditions.[54]

Interestingly, when WBCs were depleted from the blood medium, there were no clear particle adhesion trends as a function of WSR or VTC modulus (Fig. 7A–C), matching the observations of particle localization. Though this result is surprising, it is key to note that WBCs will always be clinically present; these experiments simply provide insight into the mechanism of hydrogel particle behavior. We determined that the presence of WBCs in the RBC-FL overall increased hydrogel MP adhesion. We hypothesize that these results are a combination of competing effects between the frequency of collisions between WBCs and particles, and the force balance of the resulting collisions. The frequency of collisions will, in part, be dependent on the RBC-FL thickness, which increases with increasing WSR.[55] A larger RBC-FL means a decrease in number of collisions given a constant number of particles and WBCs. Following a collision, the displacement of the colliding cell and particle will be dependent on the moduli, relative size of the two bodies, and the momentum involved in the collision. At low shear, the momentum of the collisions is not enough to produce differences in final particle adhesion to inflamed ECs compared to whole blood experiments. At intermediate WSR, collisions between more rigid hydrogels and WBCs result in larger lateral displacements towards the vessel wall, thus evening out overall adhesion in whole blood. At 1,000 s^{-1} WSR, the RBC-FL is largest, producing fewer collisions between particles and cells. Additionally, both the cells and particles have maximal momentum, resulting in larger translational displacements following each collision. As this transition to higher shear occurs, the increased displacement becomes a benefit for

all hydrogel particles, but exceptionally more so for the rigid particles. More rigid particles conserve kinetic energy best and have the most elastic collisions. Though we showed that lower moduli particles do not significantly deform under fluid shear, they still produce more inelastic collisions due to viscous energy dissipation, and therefore, displace less efficiently to the vascular wall for targeted particle adhesion. Future analysis, including a computational evaluation of cell-particle collisions within the RBC-FL, are needed to verify the details of this mechanism; however, our data clearly support the hypothesis that collisions with WBCs can contribute to 2 μm particle adhesion as a function of the particle modulus.

CONCLUSION

This work presents a comprehensive study of the role that particle modulus and size play on key transport mechanisms required for targeted particle adhesion with direct applications in VTC systems. Specifically, we show that deformable MPs are more efficient than NPs in all *in vitro* and *in vivo* experimental conditions, regardless of modulus. The presented data show that for our particle conditions A–D, there is a small difference in particle deformation under prescribed shear forces, no detectable change in particle localization to the vascular wall, and relatively linear rate of attachments. Importantly, the presence of collisions with WBCs in the RBC-FL has a dramatic role in particle lateral margination, contact with the wall, and subsequent adhesion. Our findings indicate that the ideal modulus is highly dependent on local WSR, and that superior particle adhesion to inflamed venous ECs *in vivo* can be achieved with low modulus, hydrogel MP VTCs. These VTCs simultaneously overcome margination limitations of NP VTCs and occlusive potential of rigid micron-sized VTCs. Hydrogel particles capable of localizing to the endothelium have implications for a wide range of applications, including cancer, inflammation, and cardiovascular disease. Furthermore, the trends of hydrogel modulus varying with local WSR offers potential for customized therapeutics, based on disease and tissue hemodynamics; using these findings, VTC modulus can be tuned to target a plaque in a high shear vessel or venous disease in a low shear vessel. This unique work stresses the importance of modulus on targeted drug delivery, and strikingly demonstrates that one physical property can greatly alter VTC success, with possible implications for a wide range of diseases.

METHODS

Study Approvals

Human blood used in all assays was obtained via venipuncture according to a protocol approved by the University of Michigan Internal Review Board (IRB-MED). Informed, written consent was obtained from all subjects prior to blood collection. Umbilical cords were obtained under IRB-MED approved human tissue transfer protocol, which is exempt from informed consent per federal exemption category #4 of the 45 CFR 46.101.(b).

Animal studies were conducted in accordance with National Institutes of Health guidelines for the care and use of laboratory animals and approved by the Institutional Animal Care and Use Committee (IACUC) of University of Michigan. C57BL/6 mice were obtained from

Jackson Laboratories. All animals were maintained in pathogen-free facilities at the University of Michigan.

Phlebotemy was performed according to IRB-MED approved protocols and in line with the WMA Declaration of Helsinki.

Particle Fabrication and Functionalization

Particles were fabricated via UV-initiated polymerization of PEGDA and CEA, as described in more detail in the SI. NeutrAvidin was covalently attached to the carboxylic acid through carboiimide chemistry. Biotinylated sialyl Lewis A (sLe^A) was then coupled as described previously.[23] Particles conjugated with sLe^A were stained with anti-CLA-APC and run via flow cytometry using to determine the number of sLe^A molecules. All particles for *in vitro* assays were matched to a density of 1,000 sites/μm^2. For *in vivo* experiments, biotinylated anti-CD62P was coupled to NeutrAvidin-coated particles, which were characterized using FITC anti-rat IgG1 for a total site density of ~30,000 anti-CD62P/μm^2.

PPFC Laminar Flow Assay

Human umbilical vein endothelial cells (HUVECs) were cultured on glass coverslips as described previously, with more detail in the SI.[56] Blood from human donors was drawn with the anticoagulant acetate citrate dextrose and stored at 37 °C until use. WBC depleted RBC+plasma medium was obtained as previously described. HUVECs on gelatin-coated coverslips were activated as previously described with IL-1β.[23] Targeted particles at a fixed concentration of 1×10^7 particles/mL (2 μm) or 1×10^8 particles/mL (500 nm) were mixed with either whole blood or RBC+plasma and then perfused through the PPFC in a laminar flow profile for 5 mins. The volumetric flow rate through the channel (Q) was controlled via a syringe pump, which dictates the WSR (γ_w, as shown in equation (3),

$$\gamma_w = \frac{6Q}{h^2 w}; s^{-1} \quad [1]$$

where h is the channel height (0.0127 cm), w the channel width (0.25 cm), and Q the volumetric flow rate (mL/sec). For rate of attachment experiments, images were collected every 30 seconds in the same location, including 5 mins of blood and particle flow, representing an attachment region, and 5 mins of buffer only flow, representing a detachment region. In buffer only flow, adherent NPs and MPs were visually counted and normalized to the HUVEC surface area, resulting in reported #particles/mm^2 for all experiments.

Intravital Fluorescent Microscopy

Visualization of mesentery vessels was performed as previously described.[57–59] Briefly, female mice (3–4 weeks) were anesthetized and a tail vein catheter placed for delivery of particles. A midline incision in the abdominal cavity allowed for exteriorization of the mouse intestines, and therefore, the mesentery connective tissue. Mice were placed on a custom-made microscope heated stage at 37°C and the mesentery was positioned on a glass

cover slip. A visual description of this process can be found in Reference 60. Imaged vessels were chosen based on size, with the diameter of veins ranging from 100 – 200 μm. Following vessel selection, local injury was induced by topical application of TNF-α (10 μL of 200 μg/mL in PBS). Particles suspended in PBS were injected 3 mins following topical TNF-α application via IV catheter and continuously imaged for another 5 mins via both brightfield and fluorescent microscopy. Particles were dosed by an equivalent mass of ~10 mg/kg. Targeted particle adhesion in mesenteric veins was visualized under a 25× oil objective using an inverted fluorescence microscope (Zeiss Axio Observer Z1 Marianas Microscope). These data were quantified by number of individually bound particles for n=4 mice and converted to ng particles/mm^2 vessel based on the calculated mass of one particle.

Finite Element Analysis (FEA)

Spherical 2 μm particle meshes were generated in SolidWorks CAD Software and exported to LISA. Material properties for each particle type were defined as in Fig. 1F, with Poisson's ratio of 0.5. Surface pressures of 8×10^{-13} N/μm^2 (corresponding WSR=200 s^{-1}), 4×10^{-12} N/μm^2 (corresponding WSR=1,000 s^{-1}), 2.5×10^{-11} N/μm^2, 1×10^{-9} N/μm^2, and 1×10^{-8} N/μm^2 were applied along the X-direction on the top and bottom face of the sphere in opposing directions, as shown in Fig. S8. The Taylor deformability parameter Δ was defined as $(D_{max}-D_{min})/(D_{max}+D_{min})$ as before.[61]

Flow Distribution Studies (Confocal)

A 100 μm Ibidi chamber was used to perfuse blood containing 1×10^7 particles/mL. An Olympus FV 1200 Confocal Microscope was used to detect the number of fluorescent particles at each designated height. Results presented are the number of detected particles, not simply the MFI.

Statistics

For all studies, all data points were included in the analyses and no outliers were excluded in calculations of means or statistical significance. Data are plotted with standard error bars and analyzed as indicated in Fig. legends. Specifics of each statistical test run are in the corresponding Fig. legends. Pound signs and asterisks indicate p values of *<0.05, **<0.01, ***<0.001 and ****<0.0001 and n.s. indicates not significant.

Supplementary Material

Refer to Web version on PubMed Central for supplementary material.

Acknowledgments

The authors acknowledge H. Safari, J. Noble, and A. Zimmerman for useful discussions and technical assistance. The authors acknowledge M. Gordon and C. Kloxin for discussions about and assistance with *in situ* rheometry. This work was funded in part by, University of Michigan President's Postdoctoral Fellowship (C.A.F.), and NIH grants T32-HL-125242 (M.B.F.), 5R03EB019180 (O.E.A. and T.F.S), R01 HL115138 (O.E.A.), HL114405 (M.H.), and GM105671 (M.H.).

References

1. Fish MB, Thompson AJ, Fromen CA, Eniola-Adefeso O. Emergence and Utility of Non-Spherical Particles in Biomedicine. Ind Eng Chem Res. 2015; 54:4043–4059. [PubMed: 27182109]
2. Albanese A, Tang PS, Chan WCW. The Effect of Nanoparticle Size, Shape, and Surface Chemistry on Biological Systems. Annu Rev Biomed Eng. 2012; 14:1–16. [PubMed: 22524388]
3. Torchilin VP. Multifunctional Nanocarriers. Adv Drug Deliv Rev. 2012; 64:302–315.
4. Brannon-Peppas L, Blanchette JO. Nanoparticle and Targeted Systems for Cancer Therapy. Adv Drug Deliv Rev. 2012; 6:206–212.
5. Sen Gupta A. Role of Particle Size, Shape, and Stiffness in Design of Intravascular Drug Delivery Systems: Insights from Computations, Experiments, and Nature. WIREs. 2016; 8:255–270.
6. Su J, Sun H, Meng Q, Yin Q, Tang S, Zhang P, Chen Y, Zhang Z, Yu H, Li Y. Long Circulation Red-Blood-Cell-Mimetic Nanoparticles with Peptide-Enhanced Tumor Penetration for Simultaneously Inhibiting Growth and Lung Metastasis of Breast Cancer. Adv Funct Mater. 2016; 26:1243–1252.
7. Anselmo AC, Zhang M, Kumar S, Vogus DR, Menegatti S, Helgeson ME, Mitragotri S. Elasticity of Nanoparticles Influences Their Blood Circulation, Phagocytosis, Endocytosis, and Targeting. ACS Nano. 2015; 9:3169–3177. [PubMed: 25715979]
8. Merkel TJ, Jones SW, Herlihy KP, Kersey FR, Shields AR, Napier M, Luft JC, Wu H, Zamboni WC, Wang AZ, Bear JE, DeSimone JM. Using Mechanobiological Mimicry of Red Blood Cells to Extend Circulation Times of Hydrogel Microparticles. Proc Natl Acad Sci U S A. 2011; 108:586–591. [PubMed: 21220299]
9. Yoo J, Chambers E, Mitragotri S. Factors That Control the Circulation Time of Nanoparticles in Blood: Challenges, Solutions and Future Prospects. Curr Pharamceutical Des. 2010; 16:2298–2307.
10. Beningo KA, Wang Y. Fc-Receptor-Mediated Phagocytosis Is Regulated by Mechanical Properties of the Target. J Cell Sci. 2002; 115:849–856. [PubMed: 11865040]
11. Geng Y, Dalhaimer P, Cai S, Tsai R, Tewari M, Minko T, Discher DE. Shape Effects of Filaments versus Spherical Particles in Flow and Drug Delivery. Nat Nanotechnol. 2007; 2:249–255. [PubMed: 18654271]
12. Mitragotri S, Lahann J. Physical Approaches to Biomaterial Design. Nat Mater. 2009; 8:15–23. [PubMed: 19096389]
13. Skotheim JM, Secomb TW. Red Blood Cells and Other Nonspherical Capsules in Shear Flow: Oscillatory Dynamics and the Tank-Treading-to-Tumbling Transition. Phys Rev Lett. 2007:98.
14. Crowl LM, Fogelson AL. Computational Model of Whole Blood Exhibiting Lateral Platelet Motion Induced by Red Blood Cells. Int j numer method biomed eng. 2010; 26:471–487. [PubMed: 21152372]
15. Kumar A, Graham MD. Mechanism of Margination in Confined Flows of Blood and Other Multicomponent Suspensions. Phys Rev Lett. 2012; 109:108102. [PubMed: 23005332]
16. Geislinger TM, Franke T. Hydrodynamic Lift of Vesicles and Red Blood Cells in Flow — from Fåhræus & Lindqvist to Microfluidic Cell Sorting. 2014; 208:161–176.
17. Dulinska I, Targosz M, Strojny W, Lekka M, Czuba P, Balwierz Walentyna, Szymonski M. Stiffness of Normal and Pathological Erythrocytes Studied by Means of Atomic Force Microscopy. J Biochem Biophys Methods. 2006; 66:1–11. [PubMed: 16443279]
18. Radmacher M, Fritz M, Kacher CM, Cleveland JP, Hansma PK. Measuring the Viscoelastic Properties of Human Platelets with the Atomic Force Microscope. Biophys J. 1996; 70:556–567. [PubMed: 8770233]
19. Kumar A, Rivera RGH, Graham MD. Flow-Induced Segregation in Confined Multicomponent Suspensions3: Effects of Particle Size and Rigidity. J Fluid Mech. 2014:423–462.
20. Haga J, Beaudoin A, White J, Strony J. Quantification of the Passive Mechanical Properties of the Resting Platelet. Ann Biomed Eng. 1998; 26:268–277. [PubMed: 9525767]
21. Namdee K, Carrasco-Teja M, Fish MB, Charoenphol P, Eniola-Adefeso O. Effect of Variation in Hemorheology between Human and Animal Blood on the Binding Efficacy of Vascular-Targeted Carriers. Sci Rep. 2015:5.

22. Lee TR, Choi M, Kopacz AM, Yun SH, Liu WK, Decuzzi P. On the near-Wall Accumulation of Injectable Particles in the Microcirculation: Smaller Is Not Better. Sci Rep. 2013; 3:2079. [PubMed: 23801070]
23. Charoenphol P, Huang RB, Eniola-Adefeso O. Potential Role of Size and Hemodynamics in the Efficacy of Vascular-Targeted Spherical Drug Carriers. Biomaterials. 2010; 31:1392–1402. [PubMed: 19954839]
24. Charoenphol P, Onyskiw PJ, Carrasco-Teja M, Eniola-Adefeso O. Particle-Cell Dynamics in Human Blood Flow: Implications for Vascular-Targeted Drug Delivery. J Biomech. 2012; 45:2822–2828. [PubMed: 23010218]
25. Namdee K, Thompson AJ, Golinski A, Mocherla S, Bouis D, Eniola-Adefeso O. In Vivo Evaluation of Vascular-Targeted Spheroidal Microparticles for Imaging and Drug Delivery Application in Atherosclerosis. Atherosclerosis. 2014; 237:279–286. [PubMed: 25286447]
26. Winter HH, Chambon F. Analysis of Linear Viscoelasticity of a Crosslinking Polymer at the Gel Point. J Rheol (N Y N Y). 1986; 30:367–382.
27. Stenekes RJ, De Smedt SC, Demeester J, Sun G, Zhang Z, Hennink WE. Pore Sizes in Hydrated Dextran Microspheres. Biomacromolecules. 2000; 1:696–703. [PubMed: 11710200]
28. Kansas G. Selectins and Their Ligands: Current Concepts and Controversies. Blood. 1996; 88:3259–3287. [PubMed: 8896391]
29. Foreman KE, Vaporciyan AA, Bonish BK, Jones ML, Johnson KJ, Glovsky MM, Eddy SM, Ward PA. C5a-Induced Expression of P-Selectin in Endothelial Cells. J Clin Invest. 1994; 94:1147–1155. [PubMed: 7521884]
30. Gao T, Hu HH. Deformation of Elastic Particles in Viscous Shear Flow. J Comput Phys. 2009; 228:2132–2151.
31. Chen Y. Intertia- and Deformation-Driven Migration of a Soft Particle in Confined Shear and Poiseuille Flow. RSC Adv. 2014; 4:17908–17916.
32. Doshi N, Zahr AS, Bhaskar S, Lahann J, Mitragotri S. Red Blood Cell-Mimicking Synthetic Biomaterial Particles. Proc Natl Acad Sci U S A. 2009; 106:21495–21499. [PubMed: 20018694]
33. Modery-pawlowski CL, Tian LL, Pan V, Sen Gupta A. Synthetic Approaches to RBC Mimicry and Oxygen Carrier Systems. Biomacromolecules. 2013; 14:939–948. [PubMed: 23452431]
34. Doshi N, Orje JN, Molins B, Smith JW, Mitragotri S, Ruggeri ZM. Platelet Mimetic Particles for Targeting Thrombi in Flowing Blood. Adv Mater. 2012; 24:3864–3869. [PubMed: 22641451]
35. Anselmo AC, Modery-Pawlowski CL, Menegatti S, Kumar S, Vogus DR, Tian LL, Chen M, Squires TM, Sen Gupta A, Mitragotri S. Platelet-like Nanoparticles: Mimicking Shape, Flexibility, and Surface Biology of Platelets to Target Vascular Injuries. ACS Nano. 2014; 8:11243–11253. [PubMed: 25318048]
36. Brown AC, Stabenfeldt SE, Ahn B, Hannan RT, Dhada KS, Herman ES, Stefanelli V, Guzzetta N, Alexeev A, Lam WA, Lyon LA, Barker TH. Ultrasoft Microgels Displaying Emergent Platelet-like Behaviours. Nat Mater. 2014; 13:1108–1114. [PubMed: 25194701]
37. Modery-Pawlowski CL, Tian LL, Pan V, Mccrae KR, Mitragotri S, Sen Gupta A. Biomaterials Approaches to Synthetic Platelet Analogs. Biomaterials. 2013; 34:526–541. [PubMed: 23092864]
38. Anselmo AC, Mitragotri S. Impact of Particle Elasticity on Particle-Based Drug Delivery Systems. Adv Drug Deliv Rev. 2016
39. Wang J, Byrne JD, Napier ME, Desimone JM. More Effective Nanomedicines through Particle Design. Small. 2011; 7:1919–1931. [PubMed: 21695781]
40. Peppas NA, Hilt JZ, Khademhosseini A, Langer R. Hydrogels in Biology and Medicine: From Molecular Principles to Bionanotechnology. Adv Mater. 2006; 18:1345–1360.
41. Knop K, Hoogenboom R, Fischer D, Schubert US. Poly(ethylene Glycol) in Drug Delivery: Pros and Cons as Well as Potential Alternatives. Angew Chemie - Int Ed. 2010; 49:6288–6308.
42. Zustiak SP, Leach JB. Hydrolytically Degradable Poly (Ethylene Glycol) Hydrogel Scaffolds with Tunable Degradation and Mechanical Properties. Biomacromolecules. 2010; 11:1348–1357. [PubMed: 20355705]
43. Hu Y, Xie J, Tong Y, Wang CH. Effect of PEG Conformation and Particle Size on the Cellular Uptake Efficiency of Nanoparticles with the HepG2 Cells. J Control Release. 2007; 118:7–17. [PubMed: 17241684]

44. Cui J, Björnmalm M, Liang K, Xu C, Best JP, Zhang X, Caruso F. Super-Soft Hydrogel Particles with Tunable Elasticity in a Microfluidic Blood Capillary Model. Adv Mater. 2014; 26:7295–7299. [PubMed: 25209733]
45. Cheuvront SN, Kenefick RW, Heavens KR, Spitz MG. A Comparison of Whole Blood and Plasma Osmolality and Osmolarity. J Clin Labratory Anal. 2014; 28:368–373.
46. Guo D, Li J, Xie G, Wang Y, Luo J. Elastic Properties of Polystyrene Nanospheres Evaluated with Atomic Force Microscopy: Size Effect and Error Analysis. Langmuir. 2014; 30:7206–7212. [PubMed: 24892186]
47. Addio SMD, Saad W, Ansell SM, Squiers JJ, Adamson DH, Herrera-alonso M, Wohl AR, Hoye TR, Macosko CW, Mayer LD, Vauthier C, Prud'homme RK. Effects of Block Copolymer Properties on Nanocarrier Protection from in Vivo Clearance. J Control Release. 2012; 162:208–217. [PubMed: 22732478]
48. Kutscher HL, Chao P, Deshmukh M, Singh Y, Hu P, Joseph LB, Reimer DC, Stein S, Laskin DL, Sinko PJ. Threshold Size for Optimal Passive Pulmonary Targeting and Retention of Rigid Microparticles in Rats. J Control Release. 2010; 143:31–37. [PubMed: 20043961]
49. Charoenphol P, Mocherla S, Bouis D, Namdee K, Pinsky DJ, Eniola-Adefeso O. Targeting Therapeutics to the Vascular Wall in Atherosclerosis-Carrier Size Matters. Atherosclerosis. 2011; 217:364–370. [PubMed: 21601207]
50. Koutsiaris AG, Tachmitzi SV, Batis N, Kotoula MG, Karabatsas CH, Tsironi E, Chatzoulis DZ. Volume Flow and Wall Shear Stress Quantification in the Human Conjunctival Capillaries and Post-Capillary Venules in Vivo. Biorheology. 2007; 44:375–386. [PubMed: 18401076]
51. Nagaoka T, Yoshida A. Noninvasive Evaluation of Wall Shear Stress on Retinal Microcirculation in Humans. Investig Ophthalmol Vis Sci. 2006; 47:1113–1119. [PubMed: 16505049]
52. Simon SI, Hu Y, Vestweber D, Smith WC. Neutrophil Tethering on E-Selectin Activates β 2 Integrin Binding to ICAM-1 Through a Mitogen-Activated Protein Kinase Signal Transduction Pathway. J Immunol. 2000; 164:4348–4358. [PubMed: 10754335]
53. Müller K, Fedosov DA, Gompper G. Understanding Particle Margination in Blood Flow – A Step toward Optimized Drug Delivery Systems. Med Eng Phys. 2016; 38:2–10. [PubMed: 26343228]
54. Marshall BT, Long M, Piper JW, Yago T, Mcever RP, Zhu C. Direct Observation of Catch Bonds Involving Cell-Adhesion Molecules. Nature. 2003; 423:190–193. [PubMed: 12736689]
55. Kim S, Ong PK, Yalcin O, Intaglietta M, Johnson PC. The Cell-Free Layer in Microvascular Blood Flow. Biorheology. 2009; 46:181–189. [PubMed: 19581726]
56. Huang RB, Eniola-Adefeso O. Shear Stress Modulation of IL-1-Induced E-Selectin Expression in Human Endothelial Cells. PLoS One. 2012; 7:1–11.
57. Wang Y, Reheman A, Spring CM, Kalantari J, Marshall AH, Wolberg AS, Gross PL, Weitz JI, Rand ML, Mosher DF, Freedman J, Ni H. Plasma Fibronectin Supports Hemostasis and Regulates Thrombosis. J Clin Invest. 2014; 124:4281–4293. [PubMed: 25180602]
58. Reheman A, Gross P, Yang H, Chen P, Allen D, Leytin V, Freedman J, Ni H. Vitronectin Stabilizes Thrombi and Vessel Occlusion but Plays a Dual Role in Platelet Aggregation. J Thromb Haemost. 2005; 3:875–883. [PubMed: 15733060]
59. Fromen CA, Fish MB, Zimmerman A, Adili R, Holinstat M, Eniola-Adefeso O. Evaluation of Receptor-Ligand Mechanisms of Dual-Targeted Particles to an Inflamed Endothelium. Bioeng Transl Med. 2016; 1:2–41.
60. Herr N, Mauler M, Bode C, Duerschmied D. Intravital Microscopy of Leukocyte-Endothelial and Platelet-Leukocyte Interactions in Mesenterial Veins in Mice. J Vis Exp. 2015:102.
61. Hsu CW, Chen YL. Migration and Fractionation of Deformable Particles in Microchannel. J Chem Phys. 2010:133.
62. Anseth K, Bowman CN, Brannon-peppas L. Mechanical Properties of Hydrogels and Their Experimental Determination. Biomaterials. 1996:17.
63. Fairbanks BD, Schwartz MP, Bowman CN, Anseth KS. Photoinitiated Polymerization of PEG-Diacrylate with Lithium Phenyl-2,4,6-Trimethylbenzoylphosphinate: Polymerization Rate and Cytocompatibility. Biomaterials. 2009; 30:6702–6707. [PubMed: 19783300]

64. Majima T, Schnabel W. Phenyl-2,4,6-Trimethylbenzoylphosphinates as Water-Soluble Photoinitiators. Generation and Reactivity of O=P(C6H5)(O-) Radical Anions. Makromol Chem. 1991; 192:2307–2315.

65. Huang ADAJ, Furie MB, Nicholson SC, Fischbarg J, Liebovitch LS, Silverstein SC. Effects of Human Neutrophil Chemotaxis Across Human Endothelial Cell Monolayers on the Permeability of These Monolayers to Ions and Macromolecules. J Cell Physiol. 1988; 135:355–366. [PubMed: 3397383]

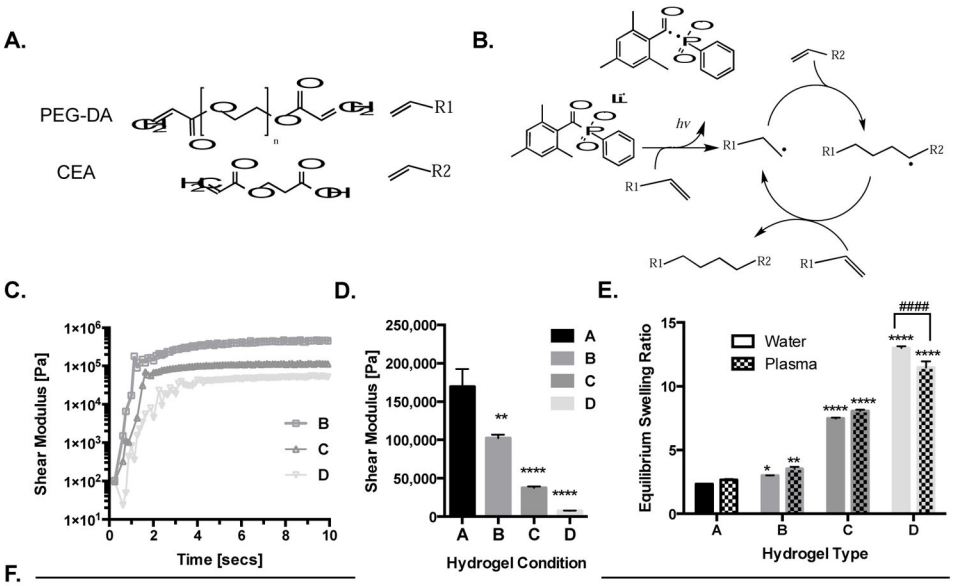

F.

Type	% Solids	% MeOH	% PEGDA	% CEA	% PI	Density (kg/m^3)	Pore Size (nm)[27]	Young's Modulus (Pa)
A	50 %	50 %	89	10	1	1051	0.376	508,300
B	40 %	60 %	89	10	1	1039	0.527	307,700
C	20 %	80 %	87	10	3	1017	1.318	113,000
D	15 %	85 %	86	10	4	1007	3.539	23,000

Figure 1. Hydrogel material properties

(A) Designation of chemical moieties for synthetic scheme. (B) Synthetic scheme for lithium phenyl-2,4,6-trimethylbenzoylphosphinate photoinitiated polymerization of (poly)ethylene glycol diacrylate (PEGDA) and 2-carboxylethyl acrylate (CEA) as described in more detail in the SI. (C) *In situ* rheometry of particle conditions B, C, and D. Condition A too rigid to be tested *in situ*. (D) Swollen shear moduli of particle conditions A–D, statistics displayed represent comparison to A. (E) Equilibrium swelling ratios of particle conditions A–D, where (*s) indicate significance within hydrogel types to A and (#s) indicate difference between water and plasma. (F) Synthesis compositions and calculated bulk material properties of hydrogels.[27] Statistical analyses were performed using one- and two-way ANOVA with Fisher's LSD test, where (*) indicates $p<0.05$, (**) indicates $p<0.01$, and (***) indicates $p<0.001$, (****) indicates $p<0.0–01$ and ($^{\#\#\#\#}$) indicates $p<0.0001$. Error bars represent standard error.

A.

Particle	Label	D Actual	PDI	ZP (mV)
A	2 μm	2.14 μm	0.11	-32.97 ± 2.01
B	2 μm	2.02 μm	0.05	-27.76 ± 0.65
C	2 μm	1.86 μm	0.14	-23.07 ± 0.60
D	2 μm	1.94 μm	0.08	-29.67 ± 0.72
A	500 nm	519.2 nm	0.21	-27.33 ± 0.96
B	500 nm	483.7 nm	0.24	-25.60 ± 0.52
C	500 nm	505.4 nm	0.14	-29.47 ± 0.91
D	500 nm	487.1 nm	0.16	-27.67 ± 0.91

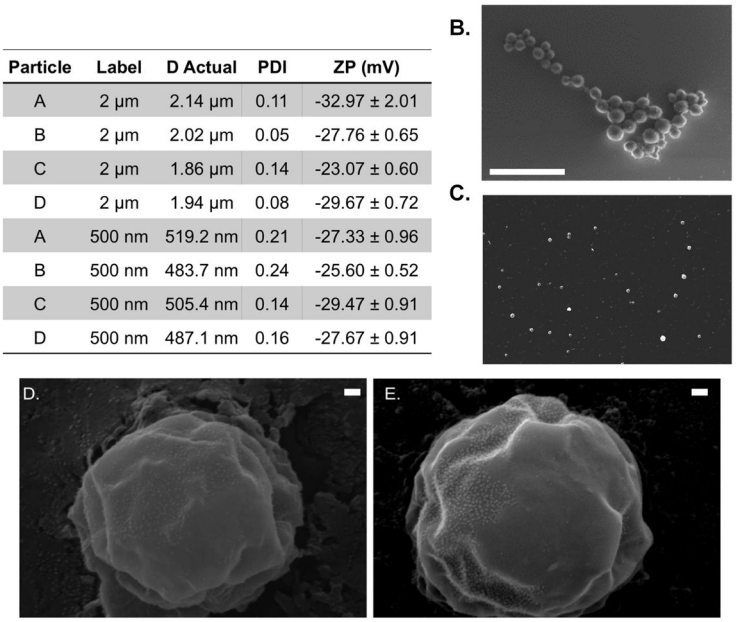

Figure 2. Hydrogel particle properties

(A) Diameter, PDI and zeta potential measurements for fabricated hydrogel particles +/− standard deviation. Representative SEM Image of dried (B) 2 μm and (C) 500 nm hydrogel condition A particles, scale bars are 5 μm. Representative scanning electron micrographs at 50,000 X magnification of (D) Hydrogel particle type A and (E) D. Scale bars are 100 nm in length.

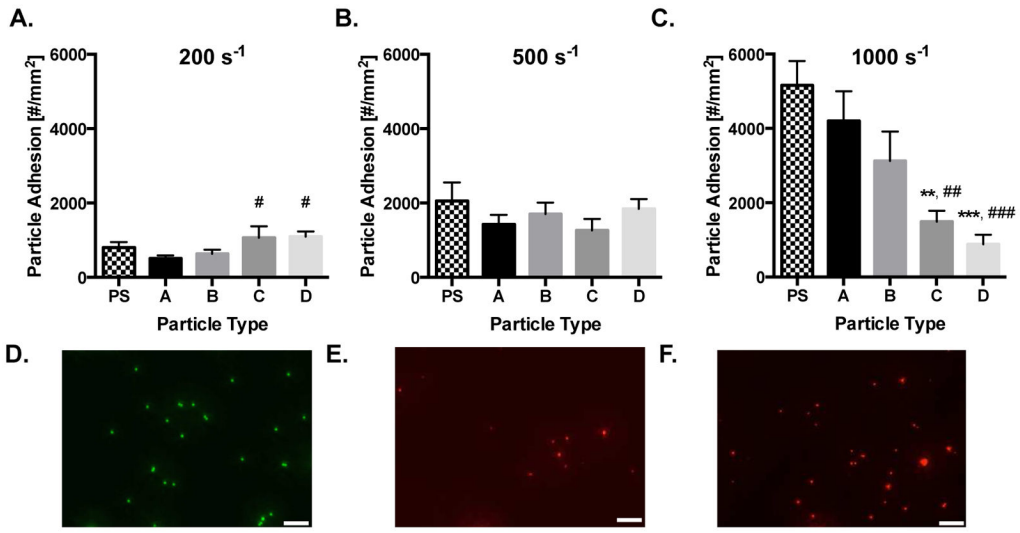

Figure 3. Particle adhesion to inflamed HUVEC monolayer as a function of particle modulus

Quantified adhesion of 2 μm hydrogel particles at a wall shear rate of (A) 200 s^{-1}, (B) 500 s^{-1}, and (C) 1,000 s^{-1} by modulus after 5 mins of laminar blood flow over an IL-1β activated HUVEC monolayer. N=3–6 human blood donors per particle condition. Statistical analysis of adherent density was performed using one-way ANOVA with Fisher's LSD test between all particle adhesion conditions. (*) Represent comparison to PS and (#) represents comparison to particle type A. (*) indicates $p<0.05$, (**) indicates $p<0.01$, and (***) indicates $p<0.001$. Error bars represent standard error. Representative fluorescent images of particles bound to IL-1β activated HUVEC under a WSR of 200 s^{-1} *in vitro* for 2 μm (D) PS, (E) Hydrogel A, and (F) Hydrogel D. Scale bars are 20 μm.

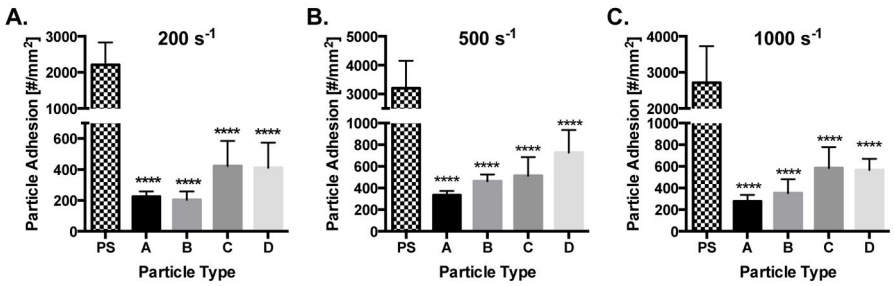

Figure 4. 500 nm particle adhesion to inflamed HUVEC monolayer as a function of particle modulus

Quantified adhesion of hydrogel particles at a wall shear rate of (A) 200 s^{-1}, (B) 500 s^{-1}, and (C) 1,000 s^{-1} by modulus after 5 mins of laminar blood flow over an IL-1β activated HUVEC monolayer at 1×10^8 particles/mL. N=3–6 human blood donors per particle condition. Statistical analysis of adherent density was performed using one-way ANOVA with Fisher's LSD test between all particle adhesion conditions. (*) Represent comparison to PS where (*) indicates $p<0.05$, (**) indicates $p<0.01$, and (***) indicates $p<0.001$. There were no significant differences amongst hydrogel particle types A–D within any wall shear rate. Error bars represent standard error.

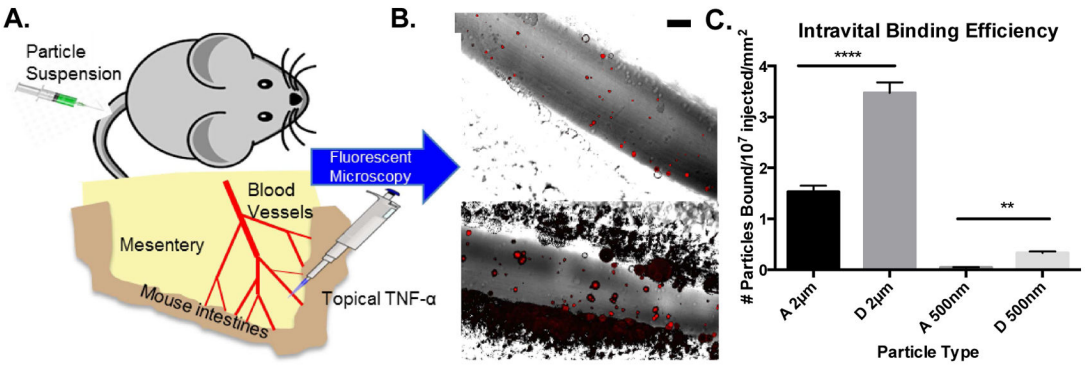

Figure 5.

Particle adhesion to inflamed mesentery endothelium as a function of modulus and size. (A) Schematic of mouse surgical technique for intravital imaging, as described in the methods. (B) Representative fluorescence images of particle adhesion to inflamed mesentery, images correspond particles A-2μm and D-2μm (top to bottom). Particle fluorescence shown in red, overlaid on the bright field image. Scale bar is 50 μm. (C) Quantified adhesion efficiency of hydrogel particle conditions A-2μm, D-2μm, A-500nm, and D-500nm, scaled by vessel area, n = 4 mice per group. Statistical analysis was performed using one-way ANOVA with Fisher's LSD test within particle sizes. (**) indicates $p<0.01$ and (****) indicates $p<0.0001$. Error bars represent standard error.

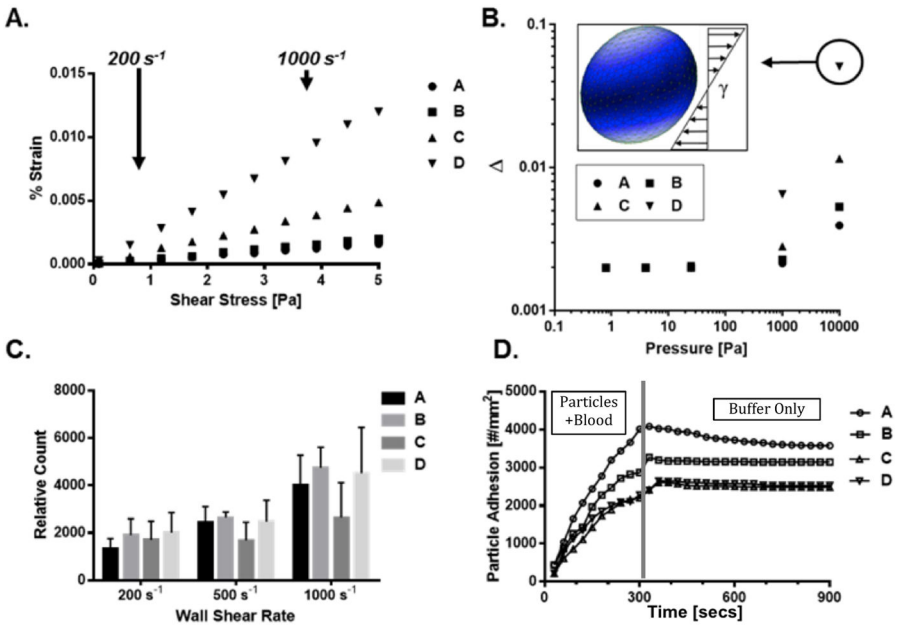

Figure 6. Hydrogel particle behavior under shear forces

(A) Strain response of bulk hydrogels A–D at controlled, applied shear stress. Arrows represent corresponding wall shear rates. (B) Deformability parameter (Δ) determined by FEA for particles A–D under a range of shear forces. Inset shows applied shear force directions and representative particle deformation of particle D under the largest shear (circled) with an amplification factor of 2 to visualize deformation. (C) Localization of fluorescent hydrogel particles from human whole blood flow to the chamber wall. N = 3 human blood donors per particle condition. Statistical analysis was performed using two-way ANOVA with Fisher's LSD test between groups, resulting in non-significant differences at all shear rates. Error bars represent the standard error. (D) Representative rate of attachment and detachment to inflamed HUVECs at wall shear rates of 1000 s^{-1}. The first 300 seconds represent perfusion of whole human blood and hydrogel particles, while the remaining time represents perfusion of buffer without particles.

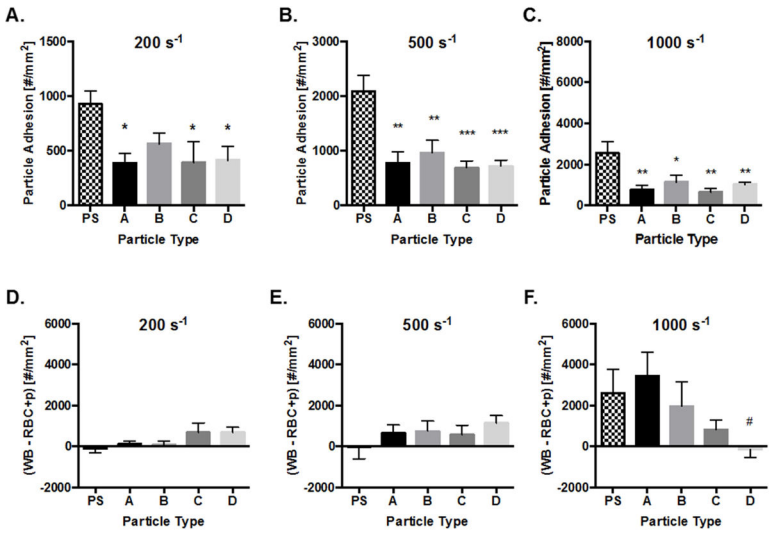

Figure 7. Particle adhesion in WBC depleted, RBC+plasma medium to inflamed HUVEC monolayer

Quantified adhesion of 2 μm hydrogel particles in RBC+plasma at a wall shear rate of (A) 200 s^{-1}, (B) 500 s^{-1}, and (C) 1,000 s^{-1} by modulus after 5 mins of laminar flow over an IL-1β activated HUVEC monolayer. N=3–6 human blood donors per particle condition in WBC depleted RBC+plasma medium. Particle adhesion in whole blood minus adhesion in RBC+plasma is quantified for (D) 200 s^{-1}, (E) 500 s^{-1}, (F) 1,000 s^{-1} by modulus. Positive values signify WBCs enhance particle binding in shear flow. Statistical analysis of adherent density was performed using one-way ANOVA with Fisher's LSD test between all particle adhesion conditions. (*) Represent comparison to PS and ($^{\#}$) represents comparison to particle type A. (*) indicates $p<0.05$, (**) indicates $p<0.01$, and (***) indicates $p<0.001$. Error bars represent standard error.